Journal of Applied Polymer Science

Optical, electrical, and electrochemical properties of graphene based water soluble polyaniline composites

Venkanna Meriga,[1] Sreeramulu Valligatla,[2] Sivaprakash Sundaresan,[3] Caroline Cahill,[4] Vinod R. Dhanak,[4] Amit K. Chakraborty[1]

[1]Carbon Nanotechnology Laboratory, Department of Physics and Centre of Excellence in Advanced Materials, National Institute of Technology, Durgapur 713209, West Bengal, India

[2]School of Physics, University of Hyderabad, 500046, India

[3]CSIR-Central Mechanical Engineering Research Institute, Durgapur 713209, West Bengal, India

[4]Department of Physics, University of Liverpool, L69 7ZE, United Kingdom

Correspondence to: A. K. Chakraborty (E-mail: amitkc61@gmail.com)

ABSTRACT: Polyaniline (PANI) is one of the most common polymers known for its conducting properties. However, poor water solubility limits its applications. In this work, PANI has been functionalized with sulfonic acid groups to produce sulfonated PANI (SPANI) offering excellent solubility in water. To compensate for the decrease of electrical conductivity due to functionalization, SPANI was combined with reduced graphene oxide (RGO) to form SPANI/RGO composites with interesting optical, thermal, and electrical properties. The composites have been characterized using X-ray diffraction (XRD), field emission scanning electron microscopy, UV–vis absorption spectroscopy, Raman spectroscopy, Fourier-transform infrared spectroscopy, X-ray photoelectron spectroscopy, thermogravimetric analysis, cyclic voltammetry, and four probe electrical conductivity measurement. The SPANI/RGO composites show increased thermal stability, reduced optical band gap and improved electrochemical properties compared with the pure polymer. © 2015 Wiley Periodicals, Inc. J. Appl. Polym. Sci. **2015**, *132*, 42766.

KEYWORDS: carbon nanotube; composites; cyclic voltammetry; electrochemical properties; Polyaniline (PANI) and SPANI; reduced graphene oxide; sulfonic acid

Received 13 March 2015; accepted 23 July 2015

DOI: 10.1002/app.42766

INTRODUCTION

Conducting polymers have been the subject of active research for the past few decades for their well-known electrical conductivity and interesting optical properties.[1,2] Polyaniline (PANI) is one of the most common conducting polymers to be investigated by researchers for its relative ease in synthesis and numerous potential applications, such as biosensors,[3,4] secondary batteries,[5,6] light-emitting diodes,[7] etc. However, a major limitation of PANI is its insolubility in common organic solvents and water.[8,9] In particular, water solubility is essential for many electrical applications. The most common method to improve the solubility and processability of PANI in water is based on sulfonation in which the emeraldine salt form of PANI is treated with chlorosulfonic acid in an inert solvent.[10,11] In this method the prepared sulfonated-PANI (SPANI) becomes water-soluble at all pH values. However, presence of the strong electron-withdrawing sulfonic acid (—SO3H) groups significantly reduces the conductivity of SPANI compared with that of pure PANI and thus limiting its electrical applications.[12,13] It is therefore, evident that an improvement in the electrical conductivity of the water-soluble SPANI is necessary to fully use the electrical properties of PANI. With this goal in mind, researchers have combined carbon nanotubes (CNTs), a nanoscale allotrope of carbon, with PANI[14–18] and SPANI[19,20] to form composites in which the idea was to exploit CNT's excellent electrical properties to increase the conductivity of the nanocomposite thus produced. Carbon based microstructures and nanostructures have also been used as reinforcement in the field of polymer nanocomposites.[21–23]

In recent years, graphene,[24] a single atomic layered sheet of carbon, has received great attention due to its outstanding electrical, mechanical, and thermal properties. Since graphene is a transparent conductor, it can be used in applications such as touch screens, light panels, and solar cells etc.[25] Other potential applications of graphene are filler material for lightweight polymer composites, field emission devices, energy storage systems, drug delivery, nanoscale electronic devices, gas sensors, etc.[26,27] High mechanical robustness, low specific mass and relatively low cost makes it ideal reinforcing candidate in polymer composites.[28]

However, due to inert nature of intrinsic graphene, it often requires some chemical/physical treatment to functionalize the surface, much like their one dimensional counterpart-CNTs.[29,30] Another advantage of using functionalized graphene is its relative ease in dispersing in solvents, which is often a necessary step for synthesis of polymer composites. The addition of graphene to a polymer remarkably improves the electrical and mechanical properties of the neat polymer matrix.[31] In particular, the combination of conducting polymers and graphene may synergistically improve the physical properties of the individual components[12,32] much like the CNTs.[33]

However, the literature shows very little work on graphene/SPANI composites. Most works have been reported on CNT/PANI and CNT/SPANI composites. For example, synthesis and characterization of externally doped SPANI/CNT composites was carried out by Lin *et al.*,[19] who concluded that CNTs could form a conducting network in well dispersed composites and could greatly increase the electrical conductivity. Wu *et al.*[17] synthesized composites of doped PANI and multiwalled CNTs (MWCNTs) via *in-situ* polymerization and observed 50–70% higher electrical conductivity. Zhang *et al.*[20] prepared a composite of functionalized MWCNTs with SPANI and observed a large increase in the solubility of the SPANI/MWCNT composites in water. Wu *et al.*[17] reported a large increase in the electrical conductivity of PANI upon addition of MWCNTs. Very recently, Bai *et al.*[34] reported the synthesis and properties of graphene/SPANI composites. The results show great promise due to improved electrical properties. However, further research is needed to better understand the underlying mechanisms and to control the properties of the composites thus produced.

We report, here, a simple solution mixing method for the synthesis of SPANI/reduced graphene oxide (RGO) composite and study its optical, thermal, and electrical properties. As synthesis of high quality graphene in large quantities is very difficult, researchers often start with graphene oxide (GO) instead of graphene and then reduce it to form RGO as an alternative to pure graphene.[26,27] We have used natural graphite to chemically synthesize GO using a modified Hummers method[35] and then reduced it to RGO during composite synthesis. We further report the non- covalent functionalization of RGO sheets by SPANI (Figure 1), to produce a water-soluble composite. Several samples were produced with different RGO concentration and were characterized using X-ray diffraction (XRD), field-emission scanning electron microscopy (FESEM), UV–vis absorption, Infrared (FTIR), X-ray photoelectron (XPS), and Raman spectroscopies. DC electrical resistance and cyclic voltammetry (CV) measurements were also carried out on these samples.

EXPERIMENTAL

Materials

All chemicals used in our experiments were reagent grade and used without further purification. Natural graphite flakes were procured from Kaiyu Industrial (HK) Limited, Nanjing, China. Sulfuric acid, Potassium permanganate, Sodium nitrate, Hydrogen peroxide, Ammonium persulfate, Aniline hydrochloride, Dichloroethane (DCE), Chlorosulfonic acid, Hydrazine hydrate, and Methanol etc. were purchased from Merck, India.

Synthesis of GO

GO was synthesized from natural graphite flakes by well-known Hummers method.[35] At first, appropriate amount of graphite powder was taken into a beaker to which appropriate amounts of conc. H2SO4 (98%) was added. The beaker was then placed in an ice bath and the whole assembly placed on a magnetic stirrer hot plate where it was stirred to mix while maintaining the temperature down to 0°C. Next, sodium nitrate and potassium permanganate were added slowly to the beaker. After 10 min, the ice-bath was removed and the temperature of the suspension was brought to room temperature by vigorously stirring the mixture for 45 min. As the reaction progressed, the mixture gradually thickened and became pasty and brownish grey in color. Water was then added drop-wise into the paste, which resulted in increase in the temperature to ~100°C. The suspension, brown in color, was further diluted with additional water after 30 min. Finally, hydrogen peroxide (30%; 20 mL) was added drop-wise into the mixture to reduce any residual permanganate. The as-produced mixture of GO and any unreacted graphite were separated through sedimentation process. Complete removal of acids was ensured by further dilution with water until pH neutral. The solution was then centrifuged at 4000 rpm for 20 min using a centrifuge (Eppendorf 5810R, Germany), and the precipitate collected from the bottom of the tubes by removing the upper liquid. Finally, the wet material was dried at 70°C in air before storing in a vacuum desiccator until further use.

Synthesis of SPANI

PANI (in emeraldine salt) was synthesized by chemical oxidation of aniline hydrochloride with ammonium persulfate at room temperature. Then appropriate quantity of aniline hydrochloride (0.2*M*) was taken into a beaker to which 100 mL of distilled water was added and sonicated for 5 min. Ammonium persulfate (0.25*M*) was taken into another beaker in which 100 mL of distilled water was added and sonicated for 5 min. The two solutions were then mixed together and polymerization was allowed for 24 h at room temperature. The mixture of green precipitate salt (PANI) was collected by filtration using a Whatman filter paper. It was then mixed with 100 mL of DCE and heated to 80°C under stirring using a magnetic stirrer (REMI 2 MLH, India). Chlorosulfonic acid solution (8 mL) diluted with DCE (16 mL) was added drop-wise during 30 min into the reaction mixture and stirred at 80°C for 1 h. This produced a semisolid precipitate, that is, SPANI to which water (50 mL) was added and heated to 60°C, and stirred for 2 h to promote hydrolysis. The resulting greenish solution was cooled to room temperature and then washed with water, followed by vacuum filtration. The filtrate was collected and dried in a vacuum desiccator until further use.

Synthesis of SPANI/RGO Composites

Homogeneous dispersions of GO were prepared by adding 30, 120, and 450 mg of GO, respectively, in 30 mL of distilled water in three beakers followed by ultrasonication for 1 h in an ultrasonic cleaner (Electro-sonic Industries, India). SPANI powder (30 mg) was added to each of the GO dispersions followed by heating for 4 h at 60°C while stirred in a magnetic stirrer to promote three SPANI/RGO composites with 50, 80, and 94%

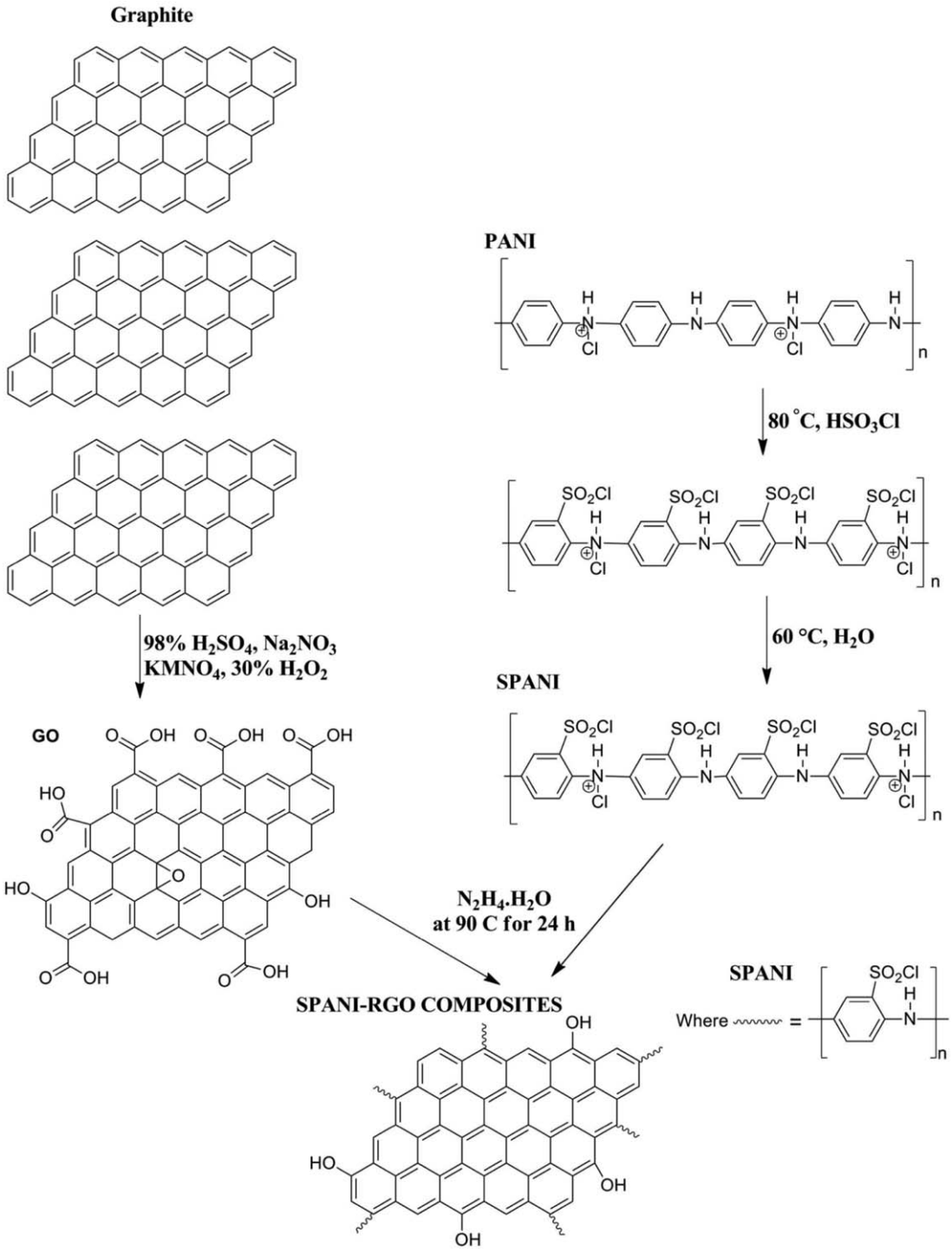

Figure 1. Schematic representation of the reaction forming SPANI/RGO composites.

RGO, respectively. The reduction of GO to RGO was achieved in the next step when hydrazine hydrate (2 mL), 32.1 mmol was added drop-wise and the solution was heated in an oil bath at 90°C under a water-cooled condenser for 24 h. Reduction of GO dispersion led to the precipitation of RGO sheets in the form of particles, and in presence of SPANI, this resulted in a homogeneous black suspension. SPANI/RGO composites were then washed with water and methanol. Then, the samples were carefully collected by filtering through a cellulose nitrate membrane (Millipore, pore size = 0.22 μm) under vacuum and subsequently dried in vacuum desiccator until further use. Three samples of SPANI/RGO composites (50, 80, and 94 wt %) were thus obtained.

Solubility Studies

The dispersions of all the samples were obtained by suspending the material (e.g., GO) in water in presence of HCl (pH was

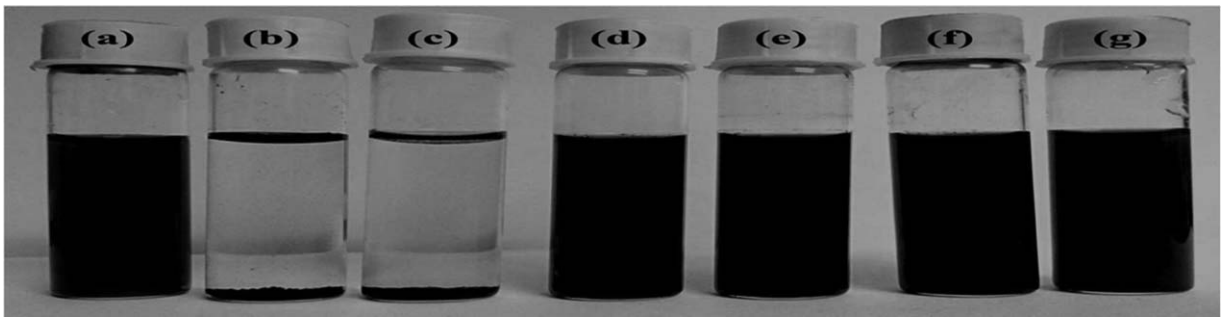

Figure 2. Photographs showing aqueous dispersions of (a) GO, (b) RGO (c) PANI, (d) SPANI, and SPANI/RGO composites containing (e) 50 wt % RGO, (f) 80 wt % RGO, and (g) 94 wt % RGO after two weeks from preparation.

adjusted to 1–2) by ultrasonication using a bath sonicator for 1 h. The vials containing the suspensions were then stored in a safe place where they were isolated against any mechanical vibration for two weeks after which the photographs of the vials were taken.

XRD Analysis

The morphology and microstructure of the samples were characterized by XRD method using a Philips Panalytical D/Max-2400 diffractometer operating with Cu $K\alpha$ radiation ($\lambda = 1.5418$ A°) at 40 kV.

UV–Visible Absorption Spectroscopy

Aqueous solutions of the samples (in 10 mm quartz cell) were characterized using an UV–vis absorption spectrophotometer (RayLeigh UV-2601, China) with 180 W operating power.

DC Electrical Measurement

The powders of SPANI/RGO composites were compressed into a pellet of 13 mm diameter. A nanovoltmeter (Keithley 2182A) and dc electrical source (Keithley 6221) were used to measure the electrical conductivity at room temperature using the standard four point probe method in a collinear geometry.

Electron Microscopy (FESEM)

Electron micrographs of the samples were recorded using a scanning electron microscope (Carl Zeiss Ultra 55, UK) equipped with a field emission gun operating at 5 KV.

Thermogravimetric Analysis

For thermal analysis, 3.5 mg of all the samples were used in a thermal analyzer [Mettler-Toledo thermogravimetric analysis (TGA)/DSC 1] at a heating rate of 20°C/min from room temperature to 800°C in nitrogen atmosphere.

Raman Spectroscopy

Raman spectra were recorded in the backscattering geometry at room temperature using a high resolution micro-Raman spectrometer (Horiba Jobin Yvon LabRam HR, France) with an Argon laser (514.5 nm) as excitation source. Calibration was performed with a silicon wafer by using the first-order phonon band of Si at 520 cm^{-1} before and after recording.

FTIR Spectroscopy

FTIR spectroscopy data were recorded using a Shimadzu IR Affinity - 1S FTIR Spectrophotometer with diamond ATR.

Photoelectron Spectroscopy

XPS measurements were performed using a Scienta SES-200 analyzer operated in ultra-high vacuum with an unmonochromated Al K_α X-ray source emitting photons of 1486.6 eV energy.

Electrochemical Measurement

The electrochemical properties of the composites were measured by CV with a potential range from −0.2 to 0.8 V using an electrochemical workstation (VSP, BioLogic, France) with Pt, Ag/AgCl and glassy carbon as counter, reference, and working electrode, respectively. Aqueous sodium sulfate solution (1*M*) was used as electrolyte. The SPANI and composite electrodes were prepared by drop casting of methanol suspension of the corresponding material on a glassy carbon electrode of 3 mm diameter, which was subsequently dried at room temperature.

RESULTS AND DISCUSSION

Figure 1 shows a schematic representation of the reactions that lead to the synthesis of SPANI/RGO composite. The two-dimensional RGO nanosheets and SPANI macromolecules interact via electrostatic interaction with the OH^- species of RGO and the $C{-}N^+$ species of SPANI.

Optical photographs of the vials containing aqueous dispersions of GO, RGO, PANI, SPANI, and SPANI/RGO composites are shown in Figure 2(a–g). It is observed that except for the samples of RGO and PANI [Figure 2(b,c)], all other suspensions [Figure 2(a,d–g)] remained stable even after two weeks as indicated by the dark solutions with no precipitation. Thus, it is evident that RGO and PANI, which are insoluble in water [as shown in Figure 2(b,c)] not only becomes soluble but also forms stable suspension over two weeks when RGO is functionalized with SPANI (to make RGO/SPANI composite). This sharp change in solution property of PANI and RGO is ascribed mainly to the electrostatic repulsion resulting from negatively charged SPANI/RGO sheets[19,34] and offers a strong support of composite formation.

Figure 3 shows the XRD data for GO, SPANI, and SPANI/RGO composites. The only peak observed for GO (curve a) is at $2\theta = 11°$ due to reflections from (0 0 2) planes of GO, which corresponds to a layer-to-layer distance (d-spacing) of 0.82 nm, much larger than that of natural graphite (0.335 nm). This increase in d-spacing is due to the interaction of water molecules and oxygen containing groups such as hydroxyl and epoxy groups on GO. Upon, reduction of GO through hydrazine hydrate treatment, the SPANI/RGO samples do not show this peak anymore while a new peak at $2\theta = 25.4°$ is observed as shown in Figure 3(curves c–e). SPANI exhibits (curve b) two characteristic peaks at $2\theta = 20°$ and 25.3° corresponding to

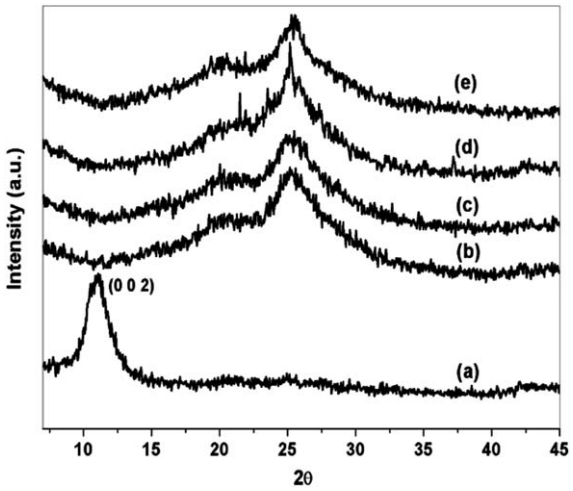

Figure 3. XRD data of (a) GO, (b) SPANI, and SPANI/RGO composites containing (c) 50 wt % RGO, (d) 80 wt % RGO, and (e) 94 wt % RGO.

reflections from (020) and (200) planes, respectively, suggesting crystalline nature of SPANI in emeraldine salt form.[36] With the incorporation of SPANI into RGO, the diffraction peaks of RGO and SPANI overlap at $2\theta = 25.4°$ resulting in a more intense and broad peak. The XRD pattern of SPANI/RGO composites (curves c–e) shows peaks related to both SPANI and RGO indicating the presence of both components in the composite.

Figure 4(A) shows the UV–vis absorption spectra in which GO exhibits (curve a) a maximum absorption peak around 228 nm, corresponding to π-π^* transition of aromatic C—C bands and a shoulder at 300 nm, due to n-π^* transitions of C═O bonds.[33] The absorption peak for RGO (curve b) is red shifted to 276 nm indicating restoration of π conjugations within the RGO nanosheets.[33] Figure 4(B) shows the UV–Visible absorption spectra of SPANI and SPANI/RGO composites. The spectrum of SPANI (curve a) has a peak at 262 nm (4.72 eV) and a shoulder peak at 452 nm (2.74 eV). The first peak arises from the π-π^* transition, which is related to conjugation length.[19,37] The second peak comes from the charged cationic species, which is known as polaron.[38] Adding 50 wt % of RGO into SPANI matrix, the absorption peak is red shifted (by 9 nm) to 271 nm (curve b). A weak peak at 371 nm is observed after doping, corresponding to the polaron transition bands and the localization of electrons in π-π^* transition.[39] With further increase in graphene content, the π-π^* transition band shows a smaller red shift (3 nm) to 265 nm compared with that of SPANI (curve c and d). The second absorption peak of SPANI/RGO composites disappear due to increased RGO content in the sample.

Because the energy gap determines the electrical conductivity and optical absorption character of a semiconductor, the energy gaps of the samples have been calculated from the absorption coefficient data. Tauc equation $[\alpha h\nu = B\ (h\nu\text{-}E_g)^n]$ has been widely used by researchers to calculate the energy band gap of bulk semiconductors, where $h\nu$ is the photon energy, h is Planck's constant, α is the absorption coefficient, E_g is the energy band gap, B is a constant, and $n = 1/2$ for direct transitions.[40] The energy band gap (E_g) is estimated by extrapolation of the tangent obtained from the plot of $(\alpha h\nu)^2$ against $(h\nu)$ as shown in Figure 5. It is to be noted that the validity of this method is somewhat limited in case of nanoparticles due to strong influence of surface states. Apart from this, the flexibility in selecting the position of the tangent in the graph allows some degree of error in measurement. Hence, the values of energy band gap obtained by this method are to be considered as rough guide only. From the intersections of the curves on X axis, as shown in Figure 5, the values of E_g have been obtained as 4.40, 2.03, 3.40 eV for GO, RGO, SPANI and 3.28, 3.12, 2.71 eV for the three SPANI/RGO composites, respectively. This is well within the expectation since oxidized graphene material (GO) is known to have poor electrical properties but when reduced to make RGO, the conductivity is expected to increase resulting in reduced band gap as seen in Figure 5(b). Because the composite samples contain RGO (not GO) in which the oxidizing groups are mostly removed, the composites of SPANI with RGO result in reduced band gap [Figure 5(b)]. Thus, we observe that the addition of RGO reduces the energy band gap of the composites compared to the pure SPANI polymer.

The four point probe (linear) electrical measurement data of SPANI gave a value of 3.2 S/cm at room temperature for the conductivity. The composite containing RGO showed gradual rise in the conductivity with increase in RGO content. The conductivity is further increased to 10.5 S/cm (three-fold increase)

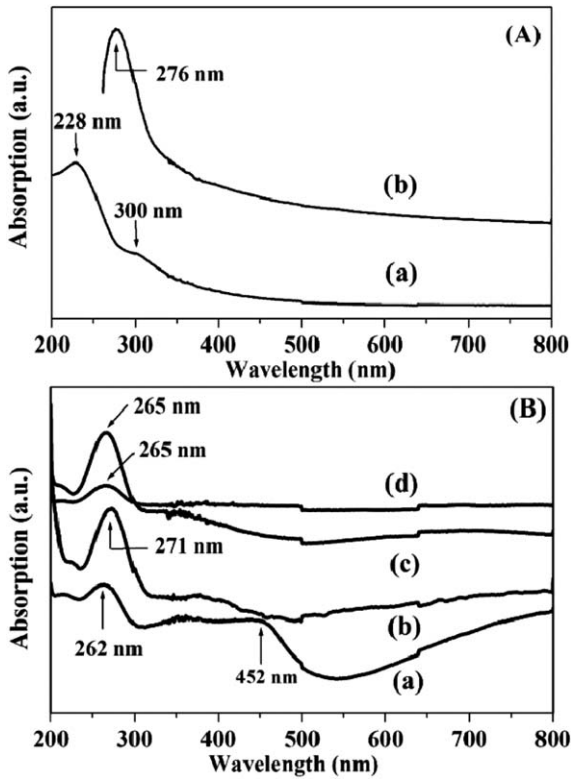

Figure 4. (A) UV–vis spectra of GO (a) and RGO (b). (B) SPANI (a), SPANI/RGO composites with 50 wt % RGO (b), 80 wt % RGO (c), and 94 wt % RGO (d).

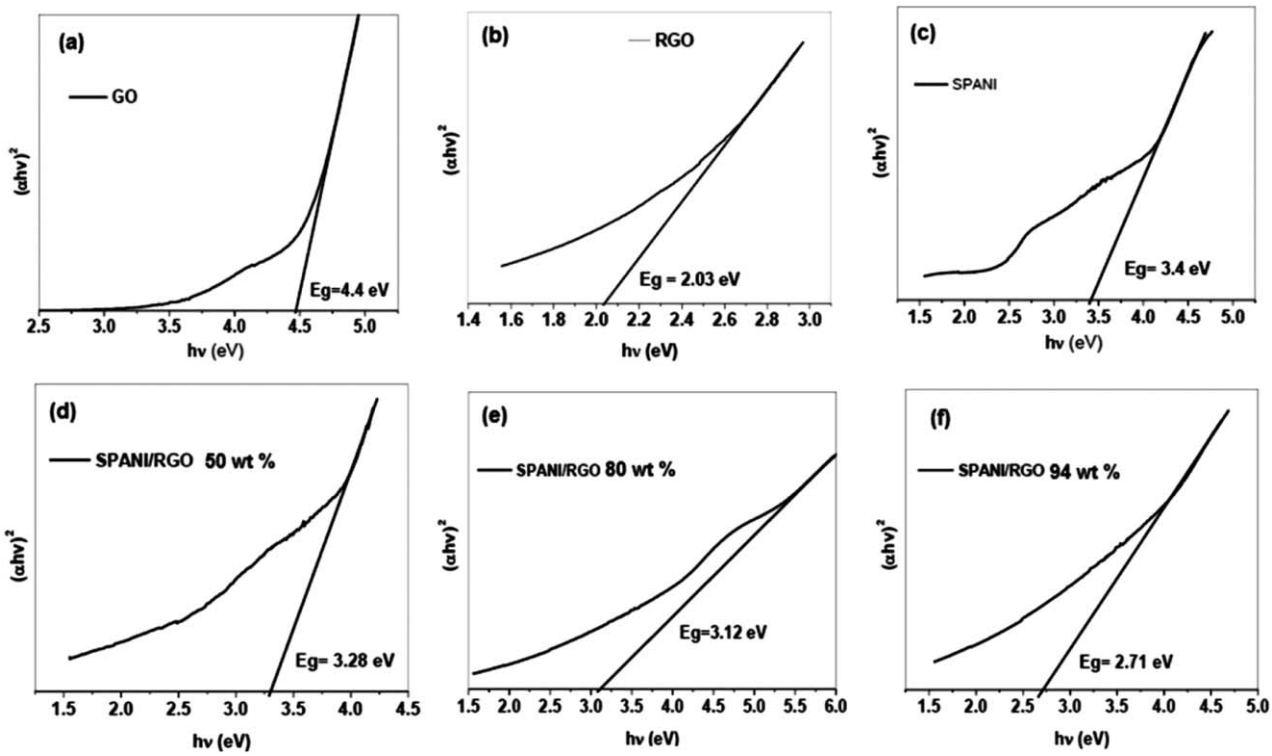

Figure 5. Plot of $(\alpha hv)2$ versus hv for GO (a), RGO (b), SPANI (c), SPANI/RGO composites with 50 wt % RGO (d), 80 wt % RGO (e), and 94 wt % RGO (f).

in the sample containing 94 wt % RGO. Thus, we see that the reduction of charge carriers in PANI due to sulfonation can be compensated by addition of RGO in these composite.

Raman spectra of the samples are shown in Figure 6. In carbon materials, it is common to observe a so-called G band, due to the E_{2g} phonon modes of sp^2 hybridized carbon atoms, and a D band due to the breathing modes of aromatic rings activated by defects.[41] Figure 6(a) shows the characteristic peak of GO at 1595 cm^{-1} (G band), which is assigned to the in-plane vibrations of the graphitic walls and the disorder-induced peak at 1353 cm^{-1} (D band) may originate from the defects in the graphitic structure.[41] The spectrum of SPANI (curve d) shows two characteristic peaks at 1341 and 1582 cm^{-1}, which are attributed to C—H bending and C═N stretching, respectively.[19,20] The spectra of the SPANI/RGO composites (curves b and c) show that the G-band of GO (1595 cm^{-1}) is shifted to lower energy (1587 cm^{-1}) due to influence of the strong C═N band of SPANI at 1582 cm^{-1} as a result of the composite formation. The graphitic G-band is shifted by about 13 cm^{-1} as a result of addition of SPANI on RGO indicating strong interaction between RGO and SPANI molecules in which RGO is coated with SPANI. There are also some fine structures around 1450 and 1500 cm^{-1} due to the C—N stretching vibration of the cation radical species.[42] The ratio of the intensity of D-to-G bands (I_D/I_G) is widely used as a measure of defect or disorder in a system. We have calculated this ratio for GO and SPANI/RGO composites (with 50 and 94 wt % of RGO) to be 0.93, 0.98, and 0.84, respectively. However, it is difficult to infer any reliable conclusion from the values as multiple vibrations of RGO and SPANI overlap in the spectrum.

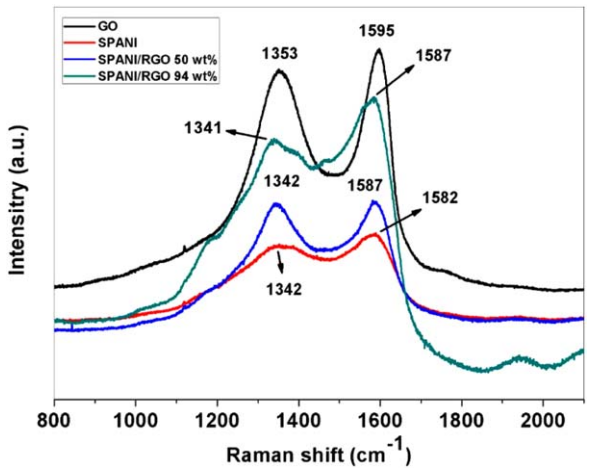

Figure 6. Raman spectra of GO (a), SPANI (b), SPANI/RGO composites with 50 wt % RGO (c), 94 wt % RGO (d). [Color figure can be viewed in the online issue, which is available at wileyonlinelibrary.com.]

Figure 7 shows FESEM images of GO and SPANI/RGO composites with 50 wt % RGO. The micrograph of GO [Figure 7(a)] clearly shows the presence of graphitic sheets whereas that of the SPANI/RGO composite [Figure 7(b)] shows many planar sheets (RGO) embedded in a granular matrix of the polymer (SPANI) suggesting a relatively good distribution of RGO in the polymer. The planar sheet structures are well separated without any observable aggregation or bunching.

Figure 8 shows the TGA plots of the samples. It is observed that GO (curve a) starts to lose mass at two different temperatures.

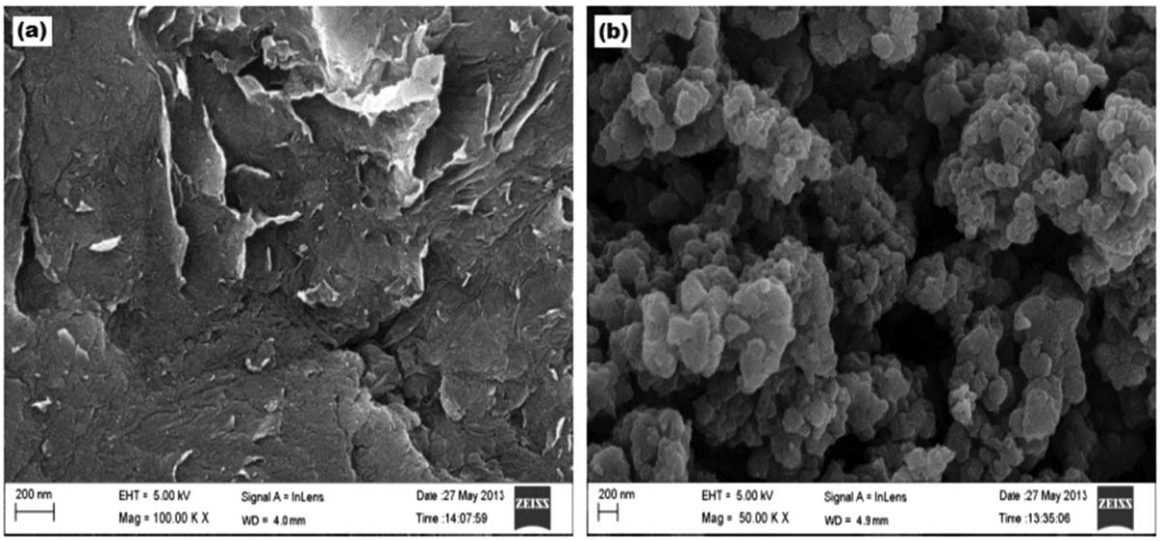

Figure 7. FESEM images of GO (a), SPANI/RGO composite containing 50 wt % RGO (b).

The first weight loss of about 10% occurs between room temperature and 100°C, which is attributed to the evaporation of any adsorbed water or other volatiles. The second weight loss of about 80% occurs at 250°C due to the decomposition of oxygen containing functional groups, yielding CO, CO_2 and steam or other oxygenated debris. The thermogram of RGO (curve f) shows a very monotonous and uniform loss of mass throughout the entire temperature region without any sharp features. For SPANI, and SPANI/RGO composites (curves b–e), the first weight loss occurs below 100°C originating from the removal of water and other volatiles. The second stage of weight loss, in the temperature range 220–350°C, is due to the decomposition of the functional groups (such as $-SO_3H$) from the polymer chains. The third stage of mass loss that occurs in the range from 350 to 800°C is due to the decomposition of the polymer backbone and their removal as carbonaceous debris. It is clearly seen that the thermograms of SPANI and SPANI/RGO composites are similar in shape but the weight losses of SPANI/RGO composites are somewhat lower than those of SPANI suggesting enhanced thermal stability of the polymer matrix by incorporation of RGO.

Figure 9 shows the FTIR spectra of GO, RGO, SPANI, and SPANI/RGO composite. While the spectrum for GO shows features at 3250 cm^{-1} (O—H stretching), 2980 cm^{-1} (C—H stretching), 1723 cm^{-1} (C=O stretching), 1632 cm^{-1} (C=C stretching), 1415 cm^{-1} (O—H deformations in the C—OH groups), 1227 cm^{-1} (C—OH stretching), and 1048 cm^{-1} (C—O stretching vibrations in C—O—C of epoxides), the spectrum for RGO is mostly flat as expected due to removal of the functional groups by reduction.[43] The FTIR spectrum of SPANI/RGO (80 wt %) composite is very similar to that of SPANI, which is not surprising since RGO does not have many active groups. The peak at 1065 cm^{-1} can be assigned to aryl-S linkages, that is, aromatic ring vibration having some C—S stretching characteristic.[44] In addition, the C—S

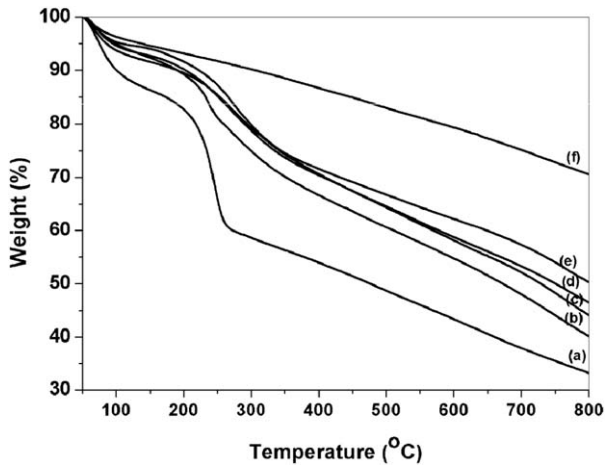

Figure 8. TGA thermograms of GO (a), SPANI (b), SPANI/RGO composites with 50 wt % RGO (c), 80 wt % RGO (d), 94 wt % RGO (e), and RGO (f).

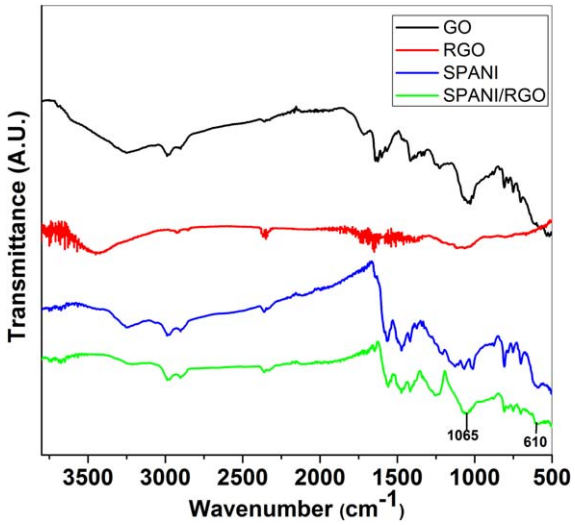

Figure 9. FTIR absorption spectra of GO, RGO, SPANI, and SPANI/RGO (80 wt %) composite. [Color figure can be viewed in the online issue, which is available at wileyonlinelibrary.com.]

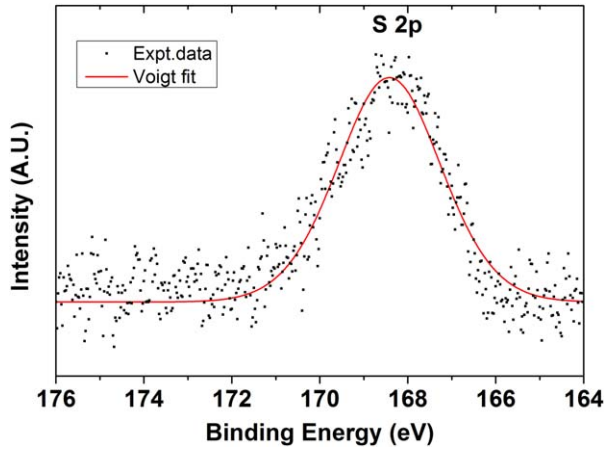

Figure 10. S 2p XPS spectrum of the SPANI/RGO (80 wt %) composite. [Color figure can be viewed in the online issue, which is available at wileyonlinelibrary.com.]

stretching vibrational mode at 610 cm^{-1} is an indicator of sulfonic acid groups' existence in SPANI and SPANI/RGO composite samples.[44]

Figure 10 shows the photoelectron spectrum obtained from the S 2p orbitals of the SPANI/RGO composite (80 wt %) sample. Due to relatively large signal-to-noise in the acquired data (scattered points), a Voigt fit is presented as a guide to the eyes (red solid line). The fitted line shows that the position of the sulfur 2p peak is at binding energy of 168.4 eV. In a similar work on CNTs functionalized with sulfonic acid groups, Adams *et al.*[45] reported a similar value of ~169 eV as the position of the S2p peak. Hence, we can conclude that the S2p peak in our work is originated from the sulfur atoms present as sulfonic acid group in the SPANI/RGO composite as there is no other source of sulfur in our composite.

Figure 11(a) compares the cyclic voltammograms obtained at a scan rate of 200 mV/s for GO, SPANI, and SPANI/RGO composite with 80 wt % RGO. The plot shows that both the peak current and the area under the curve increase for the composite samples compared with that of SPANI. It is interesting to note that the oxidation and reduction peaks expected from SPANI are not seen in the CV curves. We are not in a position at present to speculate its cause as we think further systematic studies at different pH is necessary to understand the origin, which will be the topic of future research. Figure 11(b) shows the cyclic voltammograms recorded at different scan rates for the composite containing 80 wt % RGO. The plot shows that as the scan rate is increased from 5 to 200 mV/s, the peak current increases as expected. The gradual shift of the curves further indicates a quasi-reversible reaction mechanism. Further, the estimated specific capacitances for SPANI, SPANI/RGO (50%), SPANI/RGO (80%), and SPANI/RGO (94%) show values of 30, 46, 72, and 120 F/g, respectively, when scanned at 5 mV/s. Thus, the specific capacitance increases as the RGO concentration increases in the composite. The large surface area of RGO together with good electrical conductivity play key role in enhancing the specific capacitance of the composites suggesting their potential use in supercapacitor applications.

CONCLUSION

Water soluble composites of SPANI and RGO have been synthesized starting from aniline monomer and natural graphite with different RGO-to-SPANI content. XRD and FESEM studies reveal the presence of graphitic sheets of RGO embedded in the polymer matrix. The optical band gap of SPANI has been found to be modified by the presence of RGO in the composite samples. The composites also show increased thermal stability compared with SPANI. Raman spectroscopy suggests strong interaction between the polymer and the RGO nanosheets resulting in shift of the G band as well as change in the D-to-G intensity ratio. FTIR spectra have shown features corresponding to stretching vibration of sulfonic acid groups in the composite samples due to SPANI. XPS investigation of the composite has detected presence of sulfur in sulfonic acid environment confirming that SPANI/RGO composite has indeed formed. CV has shown increased charge storage capacity of the composites compared with pure polymer (SPANI), which may be useful for energy storage applications. Thus, in this work, we have developed novel composites with interesting optical, electrical, thermal, and electrochemical properties potentially suitable for various applications using simple chemicals such as natural graphite and aniline monomer.

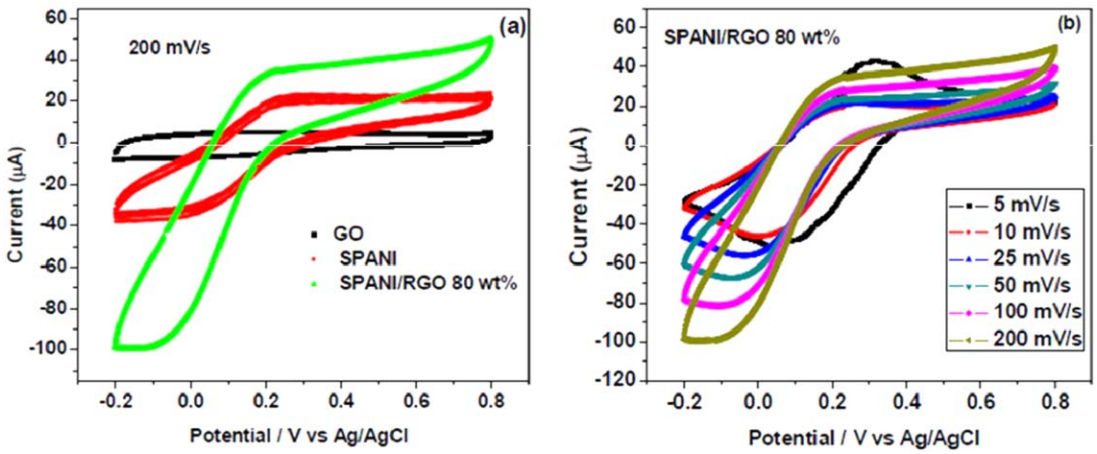

Figure 11. Cyclic voltammograms (CV) for GO, SPANI, and SPANI/RGO composite (80 wt % RGO) at fixed scan rate of 200 mV/s (a), and for SPANI/RGO composite (80 wt % RGO) at different scan rates (b). [Color figure can be viewed in the online issue, which is available at wileyonlinelibrary.com.]

ACKNOWLEDGMENTS

Dr. Subhratanu Bhattacharya and the DST-FIST facility at the Department of Physics, University of Kalyani is acknowledged for the FTIR data. AKC acknowledges the partial financial support of the Centre of Excellence grant, the MHRD, Govt. of India.

REFERENCES

1. Moliton, A.; Hiornns, R. C. *Polym. Int.* **2004**, *53*, 1397.
2. Bhattacharya, A.; De, A. *Prog. Solid State Chem.* **1996**, *24*, 141.
3. Tahir, Z. M.; Alocilja, E. C. *Biosens. Bioelectron.* **2005**, *20*, 1690.
4. Trojanowicz, M.; Geschke, O.; Krawcznski, T.; Krawczyk, V.; Cammann, K. *Sens. Actuators B* **1995**, *28*, 191.
5. Ryu, K. S.; Kim, K. M.; Kang, S. G.; Lee, G. J.; Joo, J.; Chang, S. H. *Synth. Met.* **2000**, *110*, 213.
6. Venkatachalam, S.; Prabhakaran, P. V. *Synth. Met.* **1998**, *97*, 141.
7. Gustafsson, G.; Cao, Y.; Treacy, G. M.; Klavetter, F.; Colaneri, N.; Heeger, A. *J. Nature* **1992**, *357*, 477.
8. Cheng, S. A.; Hwang, G. W. *J. Am. Chem. Soc.* **1995**, *117*, 10055.
9. Takahashi, K.; Nakamura, K.; Yamaguchi, T.; Komura, T.; Ito, S.; Aizawa, R.; Murata, K. *Synth. Met.* **2002**, *128*, 27.
10. Ito, S.; Murata, K.; Teshima, S.; Aizawa, R.; Asako, Y.; Takahashi, K. *Synth. Met.* **1998**, *96*, 161.
11. Yue, J.; Wang, Z. H.; Cromack, K. R.; Epstein, A. J.; MacDiarmid, A. G. *J. Am. Chem. Soc.* **1991**, *113*, 2665.
12. Malinauskas, A.; Malinauskiene, J.; Ramanavicius, A. *Nanotechnology* **2005**, *16*, R51.
13. Ramamurthy, P. C.; Malshe, A. M.; Harrell, W. R.; Greqory, R. V.; McGuire, K.; Rao, A. M. *Solid-State Electron.* **2004**, *48*, 2019.
14. Wu, T. M.; Lin, Y. W. *Polymer* **2006**, *47*, 3576.
15. Moniruzzaman, M.; Winey, K. I. *Macromolecules* **2006**, *39*, 5194.
16. Yuan, N. Y.; Ma, F. F.; Fan, Y.; Liu, Y. B.; Ding, J. N. *Compos. A* **2012**, *43*, 2183.
17. Wu, T. M.; Lin, Y. W.; Liao, C. S. *Carbon* **2005**, *43*, 734.
18. Goswami, S.; Maiti, U. N.; Maiti, S.; Nandy, S.; Mitra, M. K.; Chattopadhyay, K. K. *Carbon* **2011**, *49*, 2245.
19. Lin, Y-W.; Wu, T-M. *Compos. Sci. Technol.* **2009**, *69*, 2559
20. Zhang, H.; Li, H. X.; Cheng, H. M. *J. Phys. Chem. B* **2006**, *110*, 9095.
21. Kuilla, T.; Bhadra, S.; Yao, D.; Kim, N. H.; Bose, S.; Lee, J. H. *Prog. Polym. Sci.* **2010**, *35*, 1350.
22. Chakraborty, A. K.; Plyhm, T.; Necola, A.; Barbezat, M.; Terrasi, G. *J. Nanoparticle Res.* **2011**, *4*, 6493.
23. Chakraborty, A. K.; Coleman, K. S. *J. Nanosci. Nanotechnol.* **2008**, *8*, 4013.
24. Geim, A. K.; Novoselov, K. S. *Nature Mater.* **2007**, *6*, 183.
25. Yanwu, Z.; Murali, S.; Cai, W.; Li, X.; Suk, J. W.; Potts, J. R.; Ruoff, R. S. *Adv. Mater.* **2010**, *22*, 3906.
26. Singh, V.; Joung, D.; Zhai, L.; Das, S.; Khondaker, S. I.; Seal, S. *Prog. Mater. Sci.* **2011**, *56*, 1178.
27. Yang, Z.; Gao, R.; Hu, N.; Chai, J.; Cheng, Y.; Zhang, L.; Wei, H.; Kong, E. S.; Zhang, Y. *Nano-Micro Lett.* **2012**, *4*, 1.
28. Ramanathan, A. A.; Abdala, S.; Stankovich, D. A.; Dikin, M.; Herrera-Alonso, R. D.; Piner, D. H.; Adamson, H. C.; Schniepp, X.; Chen, R. S.; Ruoff, S. T.; Nguyen, I. A.; Aksay, R. K.; Prud'homme, L. C. Brinson. *Nature Nanotech.* **2008**, *3*, 327.
29. Chakraborty, A. K.; Coleman, K. S.; Dhanak, V. R. *Nanotechnology* **2009**, *20*, 155704.
30. Coleman, K. S.; Chakraborty, A. K.; Bailey, S. R.; Sloan, J.; Alexander, M. *Chem. Mater.* **2008**, *19*, 1076.
31. Coleman, J. N.; Khan, U.; Blau, W. J.; Gun'ko, Y. K. *Carbon* **2006**, *44*, 1624.
32. Baibarac, M.; Gomez-Romero, P. *J. Nanosci. Nanotech.* **2006**, *6*, 1.
33. Agrawalla, R. K.; Paul, S.; Sahoo, P. K.; Chakraborty, A. K.; Mitra, A. K. *J. Appl. Polym. Sci.* **2015**, *132*, 41692.
34. Bai, H.; Xu, Y.; Zhao, L.; Li, C.; Shi, G. *Chem. Commun.* **2009**, 1667.
35. Hummers, W. S.; Offerman, R. E. *J. Am. Chem. Soc.* **1958**, *80*, 1339.
36. Dhibar, S.; Bhattacharya, P.; Hatui, G.; Shoo, S.; Das, C. K. *ACS Sustainable Chem. Eng.* **2014**, *2*, 1114.
37. Yang, J.; Gunasekaran, S. *Carbon* **2013**, *51*, 36.
38. Stejskal, J.; Kratochvil, P.; Radhakrishnan, N. *Synth. Met.* **1993**, *61*, 225.
39. Huang, X.; Hu, N.; Gao, R.; Yu, Y.; Wang, Y.; Yang, Z. S.-W.; Kong, E.; Wei, H.; Zang, Y. *J. Mater. Chem.* **2012**, *22*, 22488.
40. Tauc, J. *Mater. Res. Bull.* **1968**, *3*, 37.
41. Konstantin, N. K.; Ozbas, B.; Schniepp, H. C.; Prud'homme, R. K.; Car, R. *Nano Lett.* **2008**, *8*, 36.
42. Al-Mashat, L.; Shin, K.; Kalantar-zadeh, K.; Plessis, J. D.; Han, S. H.; Kojima, R. W.; Kanar, R. B.; Li, D.; Gou, X.; Ippolito, S. J.; Wlodarski, W. *J. Phys. Chem. C* **2010**, *114*, 16168.
43. Wu, N.; She, X.; Yang, D.; Wu, X.; Su, F.; Chen, Y. *J. Mater. Chem.* **2012**, *22*, 17254.
44. Wei, X.-L.; Wang, Y. Z.; Long, S. M.; Bobeczko, C.; Epstein, A. J. *J. Am. Chem. Soc.* **1996**, *118*, 2545.
45. Adams, L.; Oki, A.; Grady, T.; McWhinney, H.; Luo, Z. *Phys. E* **2009**, *41*, 723.